J|A|C|S ARTICLES

Published on Web 02/10/2010

Magnetic Behavior of Odd- and Even-Electron Metal Carbonyl Clusters: The Case Study of $[Co_8Pt_4C_2(CO)_{24}]^{n-}$ ($n = 1, 2$) Carbide Cluster

Cristina Femoni,[†] Maria Carmela Iapalucci,[†] Giuliano Longoni,[†] Joanna Wolowska,[‡] Stefano Zacchini,*[,†] Piero Zanello,[§] Serena Fedi,[§] Mauro Riccò,[||] Daniele Pontiroli,[||] and Marcello Mazzani[||]

Dipartimento di Chimica Fisica e Inorganica, Università di Bologna, Viale Risorgimento 4-40136 Bologna, Italy, EPSRC Multi-Frequency EPR Centre, School of Chemistry, The University of Manchester, Oxford Road, Manchester M13 9PL, U.K., Dipartimento di Chimica, Università di Siena, Via De Gasperi 2, Siena, Italy, and Dipartimento di Fisica, Università di Parma, Via G. Usberti 7/a, Parma, Italy

Received September 8, 2009; E-mail: zac@ms.fci.unibo.it

Abstract: The reaction of $[Co_6C(CO)_{15}]^{2-}$ with 2 equiv of $PtCl_2(Et_2S)_2$ affords the new heterobimetallic $[Co_8Pt_4C_2(CO)_{24}]^{2-}$, **[1]**$^{2-}$, carbonyl cluster. **[1]**$^{2-}$ undergoes reversible chemical and electrochemical oxidation and reduction processes disclosing a complete series of **[1]**$^{n-}$ ($n = 1-4$) clusters. The mono- and dianion of **[1]**$^{n-}$ have been isolated as their tetra-substituted ammonium salts and fully characterized by means of IR, ^{13}C NMR, ESI-MS, and X-ray crystallography. Variable-temperature (VT) solid-state EPR studies on pure crystalline samples indicate that both **[1]**$^{2-}$ and **[1]**$^{-\bullet}$ are paramagnetic, due to a doublet state of the latter and a triplet state of **[1]**$^{2-}$. This conclusion is supported by SQUID measurements on the same crystalline sample of **[1]**$^{2-}$. The present study indisputably demonstrates that even-electron transition metal carbonyl clusters (TMCC) can be magnetic.

1. Introduction

The magnetic behavior of even-electron transition metal carbonyl clusters (TMCC) is controversial.[1] Insurgence of a temperature-dependent (Curie) paramagnetism resulting from quantum size effects was predicted as soon as the HOMO−LUMO gap would reduce to values close to kT.[2] Starting from experimental detection of magnetism in osmium carbonyl clusters,[3] several other molecular TMCCs have been investigated both by EPR spectroscopy[4−6] and magnetic susceptibility measurements.[1,7] Microcrystalline samples of several homometallic carbonyl clusters of ruthenium, osmium, nickel, platinum, as well as bimetallic Ni−Pt carbonyl clusters[1,6,7] revealed weak Curie-type temperature-dependent paramagnetism (TDP) corresponding to magnetic moments in the range of 0.1−4 μ_B per cluster ion, in some cases also associated with a temperature-independent (Van Vleck) paramagnetism (TIP), which was found to increase with cluster size.

However, SQUID measurements on a single crystal of $[HNi_{38}Pt_6(CO)_{48}]^{5-}$ failed to confirm the Curie-type TDP.[8] Moreover, combined magnetic susceptibility and EPR studies on single crystals of $[Fe_3Pt_3(CO)_{15}]^{2-}$ and $[Ag_{13}Fe_8(CO)_{32}]^{3-}$ salts unambiguously showed that their TDP was due to impurities of their, respectively, oxidized and reduced $[Fe_3Pt_3(CO)_{15}]^{-\bullet}$ and $[Ag_{13}Fe_8(CO)_{32}]^{4-\bullet}$ species. That stressed the necessity to investigate such a behavior by two complementary techniques, at least in those cases where the hyperfine pattern of their EPR signals (coupling of unpaired electrons of the above, respectively, with ^{195}Pt and $^{107/109}Ag$) represents a fingerprint of the odd-electron compounds.[9] Besides, DFT calculations on *optimized model structures* of highest nuclearity Ni and Ni−Pt carbonyl clusters suggested that the surface carbonyl ligands should completely quench the magnetic moments of their corresponding bare metal kernels.[10] Finally, local density functional (LDF) calculations pointed out the singlet nature of the ground states of $[M_{10}C(CO)_{24}]^{2-}$ (M = Ru, Os). Their first excited triplet state is 0.99 (Ru) and 1.23 eV

[†] Università di Bologna.
[‡] The University of Manchester.
[§] Università di Siena.
[||] Università di Parma.

(1) Cifuentes, M. P.; Humphrey, M. G.; McGrady, L. E.; Smith, P. J.; Stranger, R.; Murray, K. S.; Moubaraki, B. *J. Am. Chem. Soc.* **1997**, *119*, 2647.
(2) Edwards, P. P.; Sienko, M. J. *Int. Rev. Phys. Chem.* **1983**, *3*, 83.
(3) Benfield, R. E.; Edwards, P. P.; Stacy, A. M. *J. Chem Soc., Chem. Commun.* **1982**, 525.
(4) Drake, S. R.; Edwards, P. P.; Johnson, B. F. G.; Lewis, J.; Marseglia, E. A.; Obertelli, S. D.; Pyper, N. C. *Chem. Phys. Lett.* **1987**, *139*, 336.
(5) Benfield, R. E. *Z. Phys.* **1989**, *D12*, 453.
(6) (a) Benfield, R. E. *J. Phys. Chem.* **1987**, *91*, 2712. (b) Johnson, D. C.; Benfield, R. E.; Edwards, P. P.; Nelson, W. J. H.; Vargas, M. D. *Nature* **1985**, *314*, 231.
(7) (a) Pronk, B. J.; Brom, H. B.; de Jongh, L. J.; Longoni, G.; Ceriotti, A. *Solid State Commun.* **1986**, *59*, 349. (b) Teo, B. K.; DiSalvo, F. J.; Waszczak, J. V.; Longoni, G.; Ceriotti, A. *Inorg. Chem.* **1986**, *25*, 2262.
(8) van Leeuwen, D. A.; van Ruitenbeek, J. M.; de Jongh, L. J.; Ceriotti, A.; Pacchioni, G.; Haberlein, O. D.; Rosch, N. *Phys. Rev. Lett.* **1994**, *73*, 1432.
(9) Sinzig, J.; de Jongh, L. J.; Ceriotti, A.; Della Pergola, R.; Longoni, G.; Stener, M.; Albert, K.; Rosch, N. *Phys. Rev. Lett.* **1998**, *81*, 3211.

(Os) higher in energy, implying a negligible occupation of that state even at room temperature.[1]

The above experimental and theoretical observations led to the conclusion that TDP, as well as TIP, of even-electron TMCC systematically arises from adventitious contamination with odd-electron species or the presence of unidentified magnetic impurities. Consequently, studies aimed at proving that large TMCCs could feature progressively vanishing HOMO−LUMO gaps and high-spin ground states as a function of size came to a rest.

A somehow related controversy regarding the magnetic properties of ligand-stabilized gold nanoparticles and thiolated gold surfaces or thin films was raised later in the literature.[11] Assessment of intrinsic magnetic properties of gold nanoparticles, rather than molecular TMCC, would be further complicated by their nonmolecular nature and ill-defined composition and structure.

More recently, DFT calculations suggested that even low nuclearity TMCCs such as $[Fe_6Ni_6N_2(CO)_{24}]^{n-}$ ($n = 2, 4$),[12] $[Co_{11}RhN_2(CO)_{24}]^{2-}$, and $[Co_{10}Rh_2N_2(CO)_{24}]^{2-}$ [13] could feature a triplet ground state, which was partially substantiated in the latter by EPR.

It was therefore of interest to find some case study where a TMCC readily obtainable in high yields and featuring a relatively small nuclearity is amenable to investigation by miscellaneous spectroscopic techniques. As a result, we here report the synthesis, structure, and chemical, electrochemical, and physical characterization of new bimetallic Co−Pt carbido carbonyl clusters, namely, $[Co_8Pt_4C_2(CO)_{24}]^{2-}$, $\mathbf{[1]^{2-}}$, and $[Co_8Pt_4C_2(CO)_{24}]^{-\bullet}$, $\mathbf{[1]^{-\bullet}}$, structurally related to the above nitrides, which indisputably demonstrate that even electron TMCCs can be magnetic. Indeed, experimental VT EPR and SQUID measurements suggest the presence of a triplet state in the even-electron $\mathbf{[1]^{2-}}$. Contamination of the $\mathbf{[1]^{2-}}$ sample by the odd-electron $\mathbf{[1]^{-\bullet}}$ is ruled out by the absence of its distinctive EPR fingerprint.

2. Results and Discussion

2.1. Synthesis and Characterization of $\mathbf{[1]^{2-}}$ and $\mathbf{[1]^{-\bullet}}$. Addition of 2 equiv of $PtCl_2(Et_2S)_2$ to a THF solution of $[Co_6C(CO)_{15}]^{2-}$ affords almost pure $\mathbf{[1]^{2-}}$ in good yields (ca. 86% based on Pt). Conversely, the addition of smaller amounts of $PtCl_2(Et_2S)_2$ (less than 2 equiv) results in the formation of $\mathbf{[1]^{2-}}$ in mixture with a new species tentatively formulated as $[Co_9Pt_3C_2(CO)_{24}]^{n-}$ ($n = 2,3$), $\mathbf{[2]^{n-}}$, on the basis of ESI-MS and electrochemical data (see Supporting Information for further details). Unfortunately, all attempts to isolate pure $\mathbf{[2]^{n-}}$ salts so far met little success. Nonetheless, further addition of $PtCl_2(Et_2S)_2$ results in the quantitative conversion of $\mathbf{[2]^{n-}}$ into $\mathbf{[1]^{2-}}$, and crystalline samples of the latter have been isolated after precipitation and crystallization from THF/*n*-hexane. The nature of the new heterometallic carbide carbonyl cluster $\mathbf{[1]^{2-}}$ and its purity have been determined by elemental analysis, IR, ^{13}C NMR, and ESI-MS. Moreover, its structure has been ascertained by X-ray crystallography on two different salts, that is, $[NMe_4]_2\mathbf{[1]}\cdot 2THF$ and $[NMe_3(CH_2Ph)]_2\mathbf{[1]}\cdot 2THF\cdot 0.5CH_3C_6H_5$.

In keeping with the carbonyl stereochemistry inferred from the X-ray structure, the green $\mathbf{[1]^{2-}}$ compound displays two bands at 2013 (s) and 1828 (m) cm^{-1} due to the presence of both terminal and bridging CO's. The cluster anions in both crystal structures are identical (see section 2.2) and display a partial Co−Pt positional disorder. The exact Co/Pt ratio has been determined by elemental analyses and ESI-MS. The ESI-MS spectra recorded on different samples of both salts systematically confirm a strict 8/4 ratio between the two metals. In particular, the mass spectra display a main set (relative intensity in parentheses) of peaks centered at *m*/*z* 974 (100) due to $\mathbf{[1]^{2-}}$ and a minor set of peaks centered at *m*/*z* 1947 (15) due to the $\mathbf{[1]^{-\bullet}}$ monoanion.

In view of the structure of $\mathbf{[1]^{2-}}$ and the observed positional disorder of the four Pt atoms, three different isomers are possible (see Figure 2): *trans*-(2 + 2), *cis*-(2 + 2) and (3 + 1). ^{13}C NMR studies on a sample of $\mathbf{[1]^{2-}}$, prepared from $[Co_6{}^{13}C(CO)_{15}]^{2-}$, show that the (3 + 1) isomer is never present. Indeed, the ^{13}C NMR spectrum of $\mathbf{[1]^{2-}}$ consists of a single nonpolynomial quintet at δ 353.9 ppm ($^1J_{Pt-C} = 396$ Hz), indicating equivalence of the two carbide atoms. Such a spectrum is only in keeping with a (2 + 2) distribution of Pt atoms.

The oxidation of $\mathbf{[1]^{2-}}$ with stoichiometric amounts of oxidizing agents, such as I_2 or Ag^+, results in the quantitative shift of its IR ν(CO) toward higher frequencies, owing to formation of the $\mathbf{[1]^{-\bullet}}$ odd-electron species. The brownish green $\mathbf{[1]^{-\bullet}}$ monoanion shows IR carbonyl absorptions at 2040 (s) and 1848 (m) cm^{-1}. The ESI-MS spectrum of its $[NMe_3(CH_2Ph)]^+$ salt in THF solution displays the same sets of peaks of the dianion but with reversed intensities [1947(100) and 974(35) *m*/*z*]. However, a third set of peaks centered at *m*/*z* 2084 (30) due to a minor $[Co_7Pt_5C_2(CO)_{24}]^-$ ($\mathbf{[3]^-}$) impurity is also present. On the basis of the intensities of the ESI-MS peaks, the $\mathbf{[1]^{-\bullet}}/\mathbf{[3]^-}$ ratio is ca. 4.5. This finding led to the question whether $\mathbf{[3]^-}$ represents a side product of the oxidation reaction, which contaminates $\mathbf{[1]^{-\bullet}}$ salts from the beginning, or it is generated by partial decomposition of $\mathbf{[1]^{-\bullet}}$ in the ESI-MS experiment. It must be emphasized that all analyses performed before chemical oxidation of $\mathbf{[1]^{2-}}$ excluded the presence of $\mathbf{[3]^-}$.

Since the identical M/charge and CO/charge ratios make the odd-electron $\mathbf{[1]^{-\bullet}}$ and the even-electron $\mathbf{[3]^-}$ monoanions indistinguishable by IR, the oxidation of $\mathbf{[1]^{2-}}$ was monitored by ^{13}C NMR using a sample of the dianion with 100% isotopically enriched ^{13}C on the carbide atoms. The spectra clearly point out that formation of $\mathbf{[1]^{-\bullet}}$ (quintet; δ 304.1 ppm, $^1J_{Pt-C} = 315$ Hz) is accompanied by minor amounts of the known $[Co_6(^{13}C)(CO)_{14}]^-$ (singlet; 389.4 ppm) and also reveal the presence of two new signals (quintet, δ 368.5 ppm $^1J_{Pt-C} = 358$ Hz; and a partially hidden multiplet at δ 388.1 ppm) which can be tentatively assigned to $\mathbf{[3]^-}$ (see Supporting Information). Incidentally, it is worth noting that the paramagnetism of all these species does not hamper observation nor significantly broaden their ^{13}C NMR spectra. Since $\mathbf{[1]^{-\bullet}}$, once isolated, is

(10) (a) Rösch, N.; Pacchioni, G. In *Clusters and Colloids: From Theory to Applications*; Schmid, G., Ed.; VCH: Weinheim, Germany, 1994; p 68. (b) Rösch, N.; Ackermann, L.; Pacchioni, G. *J. Am. Chem. Soc.* **1992**, *114*, 3549. (c) Rösch, N.; Ackermann, L.; Pacchioni, G.; Dunlap, B. I. *J. Chem. Phys.* **1991**, *95*, 7004. (d) Pacchioni, G.; Rösch, N. *Acc. Chem. Res.* **1995**, *28*, 390.

(11) (a) Crespo, P.; Litràn, R.; Rojas, T. C.; Multigner, M.; de la Fuente, J. M.; Sànchez-Lopez, J. C.; Garcìa, M. A.; Hernando, A.; Penadés, S.; Fernàndez, A. *Phys. Rev. Lett.* **2004**, *93*, 087204-1–087204-4. (b) Iwasa, T.; Nobusada, K. *Chem. Phys. Lett.* **2007**, *441*, 268. (c) Negishi, Y.; Tsunoyama, H.; Suzuki, M.; Kawamura, N.; Matsushita, M. M.; Maruyama, K.; Sugawara, T.; Yokoyama, T.; Tsukuda, T. *J. Am. Chem. Soc.* **2006**, *128*, 12034, and references cited therein.

(12) Della Pergola, R.; Bruschi, M.; Fabrizi de Biani, F.; Fumagalli, A.; Garlaschelli, L.; Laschi, F.; Manassero, M.; Sansoni, M.; Zanello, P. *C.R. Chimie* **2005**, *8*, 1850.

(13) Costa, M.; Della Pergola, R.; Fumagalli, A.; Laschi, F.; Losi, S.; Macchi, P.; Sironi, A.; Zanello, P. *Inorg. Chem.* **2007**, *46*, 552.

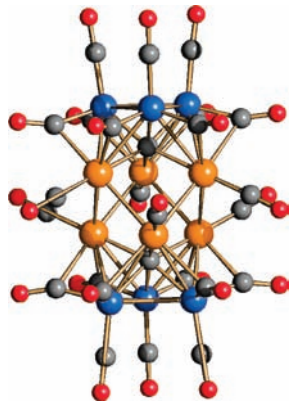

Figure 1. Molecular structure of $[\mathbf{1}]^{n-}$ (n = 1, 2). Co, blue spheres; disordered Co/Pt, orange; C, gray; and O, red.

stable for days, these ^{13}C NMR data make it more likely that $[\mathbf{3}]^-$ is concomitantly obtained with $[\mathbf{1}]^{-\bullet}$ during the oxidation of $[\mathbf{1}]^{2-}$.

The $[Co_6C(CO)_{14}]^-$ salts can be eliminated from the reaction mixture by crystallization of the crude material obtained by evaporation of the reaction solution, while $[\mathbf{1}]^{-\bullet}$ and $[\mathbf{3}]^-$ as their $[NMe_3(CH_2Ph)]^+$ salts cocrystallize by virtue of their very similar structure and identical charge.

The structure of the above cocrystallized mixture of monoanions has been fully elucidated by X-ray crystallography of the $[NMe_3(CH_2Ph)][Co_{8-x}Pt_{4+x}C_2(CO)_{24}]$ (x = 0,1) salt (section 2.2) and is substantially identical to that of the $[\mathbf{1}]^{2-}$ dianion.

The chemical reduction of $[\mathbf{1}]^{2-}$ in THF solution with Na/naphthalene proceeds via the formation of a first brown $[\mathbf{1}]^{3-}$ product, which displays carbonyl IR absorptions at 1988 (s) and 1812 (br) cm^{-1}. The reaction is perfectly reversible, and the green dianion $[\mathbf{1}]^{2-}$ is quantitatively restored by controlled oxidation with air. Further addition of Na/naphthalene to the solution of $[\mathbf{1}]^{3-}$ results in the formation of a more reduced species displaying ν(CO) at 1965 (s) and 1799 (br) cm^{-1}, which may be confidently attributed to the $[\mathbf{1}]^{4-}$ tetra-anion. Both of these reduced species are very reactive, and this hindered their isolation in a pure state and crystallization. Notably, the formulations of above species as $[\mathbf{1}]^{3-}$and $[\mathbf{1}]^{4-}$ are also supported by the electrochemical experiments reported in section 2.3.

2.2. Crystal Structures of $[NMe_4]_2[\mathbf{1}]\cdot 2THF$, $[NMe_3(CH_2Ph)]_2[\mathbf{1}]\cdot 2THF\cdot 0.5CH_3C_6H_5$, and $[NMe_3(CH_2Ph)][Co_{8-x}Pt_{4+x}C_2(CO)_{24}]$ (x = 0, 1). The molecular structure of the dianion $[\mathbf{1}]^{2-}$ has been determined on both $[NMe_4]_2[\mathbf{1}]\cdot 2THF$ and $[NMe_3(CH_2Ph)]_2[\mathbf{1}]\cdot 2THF\cdot 0.5CH_3C_6H_5$ salts, in order to better elucidate the Co−Pt disorder present in the cluster. The overall composition [Co/Pt = 8/4] has been imposed on the basis of elemental and ESI-MS analyses performed on different batches of crystals and used as restraint during the refinement.

In the case of $[NMe_4]_2[\mathbf{1}]\cdot 2THF$, the unit cell contains four cluster anions (located on an inversion center; therefore, only half of the atoms are independent), eight $[NMe_4]^+$ cations, and eight THF molecules. Conversely, the unit cell of $[NMe_3(CH_2Ph)]_2[\mathbf{1}]\cdot 2THF\cdot 0.5CH_3C_6H_5$ contains four cluster anions, eight $[NMe_3(CH_2Ph)]^+$ cations, eight THF molecules (all located on general positions), and two toluene molecules (located on an inversion center).

The molecular structure of the dianion $[\mathbf{1}]^{2-}$ (Figure 1 and Table 1) closely resembles those previously reported for $[Co_{10}Rh_2N_2(CO)_{24}]^{2-}$, $[Co_{11}RhN_2(CO)_{24}]^{2-}$,[13] and $[Fe_6Ni_6N_2(CO)_{24}]^{n-}$ (n = 2−4).[12] Thus, its metal cage consists on a face-sharing trioctahedron of idealized D_{3d} symmetry. This derives from a hexagonal close-packed fragment containing an *abab* stacking of four triangles. On both salts, the six positions of the two outer triangles are occupied exclusively by Co atoms, whereas the six inner positions, corresponding to the central octahedron, are disordered Pt and Co sites. Due to the presence of an inversion center on the cluster anion of $[NMe_4]_2[\mathbf{1}]\cdot 2THF$, its structure is not very informative on this point.

Conversely, analysis of the occupancy factors of $[NMe_3(CH_2Ph)]_2[\mathbf{1}]\cdot 2THF\cdot 0.5CH_3C_6H_5$, where all metal atoms are independent, indicates that for two positions (one per inner triangle in a relative *trans* position) the Pt occupancy factors [M(5) 0.47164, M(6) 0.30775] are considerably smaller than for the other four positions [M(1) 0.85510, M(2) 0.83742, M(3) 0.79170, M(4) 0.73567] (see Supporting Information for labeling).

In distributing the four Pt atoms over the central octahedron, three different isomers are, in principle, possible (Figure 2). A first isomer could have three Pt atoms located in one inner triangle and a fourth in the other one [isomer (3 + 1)]. The other two possible isomers would have two Pt atoms on each of the two inner triangles, in a relative *cis* [*cis*-(2 + 2)] or *trans* [*trans*-(2 + 2)] position. ^{13}C NMR studies (section 2.1) clearly indicate that only a (2 + 2) isomer is present owing to the equivalence of the two interstitial carbide atoms with a likely predominance of the *trans*-(2 + 2) on the *cis*-(2 + 2) isomer. The above-mentioned Pt occupancy factors can then be justified by association in the crystal of (2 + 2) isomers in three different orientations around the pseudo-C_3 axis, giving rise to either complete or partial Co/Pt randomization in the $[NMe_4]^+$ and $[NMe_3CH_2Ph]^+$ salts, respectively.

The two carbide atoms are located in the outer octahedra and displaced from the center toward the inner triangles. The Co−C carbide distances (average 1.97 Å in both salts) are longer than in the octahedral paramagnetic $[Co_6C(CO)_{14}]^-$ (average 1.88 Å)[14] and comparable to the ones found in larger cages such as trigonal prismatic, $[Co_6C(CO)_{15}]^{2-}$ (average 1.96 Å)[15] and $[Co_{13}C_2(CO)_{24}]^{4-}$ (average 1.98 Å),[16] or square antiprismatic, $[Co_8C(CO)_{18}]^{2-}$ (average 2.07 Å).[17] This is probably a consequence of the swelling of the octahedral cage in $[\mathbf{1}]^{2-}$ due to the presence of the larger Pt atoms and the electron richness of the cluster (vide infra). The even longer M−C distances with the inner triangles (average 2.02 and 2.07 Å for the two salts, respectively) are also a consequence of the presence of disordered Pt atoms.

Concerning the M−M interactions, four different sets can be identified: the intratriangle distances in the inner (I) and outer (II) triangles, the intertriangle distances between the inner and the outer triangles (III), and between the two inner triangles (IV). Distances of types (II), (III), and (IV) are in the normal ranges for Co−Co and Co−Pt bonding contacts and do not deserve any particular comment.

(14) (a) Albano, V. G.; Chini, P.; Ciani, G.; Sansoni, M.; Strumolo, D.; Heaton, B. T.; Martinengo, S. *J. Am. Chem. Soc.* **1976**, *98*, 5027. (b) Albano, V. G.; Chini, P.; Ciani, G.; Sansoni, M.; Martinengo, S. *J. Chem. Soc., Dalton Trans.* **1980**, 163.
(15) (a) Albano, V. G.; Chini, P.; Martinengo, S.; Sansoni, M.; Strumolo, D. *J. Chem. Soc., Dalton Trans.* **1974**, 299. (b) Martinengo, S.; Strumolo, D.; Chini, P.; Albano, V. G.; Braga, D. *J. Chem. Soc., Dalton Trans.* **1985**, 35.
(16) Albano, V. G.; Braga, D.; Chini, P.; Ciani, G.; Martinengo, S. *J. Chem. Soc., Dalton Trans.* **1982**, 645.
(17) Albano, V. G.; Chini, P.; Ciani, G.; Martinengo, S.; Sansoni, M. *J. Chem. Soc., Dalton Trans.* **1978**, 463.

Table 1. Main Bond Distances (Å) for $[1]^{n-}$ ($n = 1, 2$)

	$[1]^{2-}$ [a]	$[1]^{2-}$ [b]	$[1]^{-\bullet}$ [c]
M−M[d] in the inner triangles (I)	3.222(2)−3.278(1) 3.20 average	3.1443(11)−3.2375(14) 3.20 average	3.1485(4)−3.257(2) 3.22 average
Co−Co in the outer triangles (II)	2.628(2)−2.640(2) 2.63 average	2.594(3)−2.631(3) 2.62 average	2.5739(13)−2.6456(10) 2.62 average
Co−M[d] in the outer (centered) octahedron (III)	2.6784(13)−2.7320(13) 2.71 average	2.638(3)−2.749(2) 2.70 average	2.6000(9)−2.7478(6) 2.68 average
M−M[d] in the inner (noncentered) octahedron (IV)	2.6947(6)−2.7222(7) 2.71 average	2.6368(12)−2.7291(17) 2.69 average	2.7269(4)−2.7555(6) 2.75 average
Co−C carbide	1.960(7)−1.993(8) 1.97 average	1.955(14)−1.989(13) 1.97 average	1.971(4)−2.002(5) 1.98 average
M−C[d] carbide	2.043(7)−2.070(18) 2.06 average	2.010(14)−2.039(14) 2.02 average	1.991(5)−2.028(3) 2.02 average

[a] As found in the $[NMe_4]_2[Co_8Pt_4C_2(CO)_{24}]\cdot 2THF$ salt. [b] As found in the $[NMe_3(CH_2Ph)]_2[Co_8Pt_4C_2(CO)_{24}]\cdot 2THF\cdot 0.5CH_3C_6H_5$ salt. [c] As found in the $[NMe_3(CH_2Ph)][Co_{8-x}Pt_{4+x}C_2(CO)_{24}]$ ($x = 0,1$) salt. [d] M refers to disordered Co and Pt.

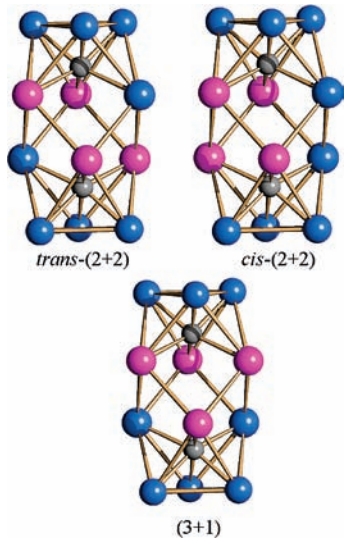

Figure 2. Three possible isomers of $[1]^{2-}$ (only the metal framework and the interstitial carbide atoms are drawn). Blue spheres represent Co, magenta spheres are Pt.

The intratriangle contacts within the inner triangles (I) are rather loose and substantially nonbonding [3.222(2)−3.278(1) Å, average 3.20 Å; 3.1443(11)−3.2375(14) Å, average 3.20 Å for the two salts, respectively], even for Pt−Pt interactions. As a comparison, the Pt−Pt bonding distances in the triangle layered $[Pt_{3n}(CO)_{6n}]^{2-}$ clusters are usually in the range of 2.65−2.70 Å for CO bridged and 3.00−3.12 Å for unbridged bonds.[18,19] The observed contacts indicate a limiting situation between bonding and nonbonding, as inferable from the values of the van der Waals radii of Pt and Co, which are accepted to fall in the 1.7−1.8 Å range. The considerable swelling of the inner triangles in $[1]^{2-}$ is probably a consequence of its electron richness. In fact, according to Mingo's rule,[20] a trioctahedral metal cluster should have 162 cluster valence electrons (CVE). Documented examples are $H_2Rh_{12}(CO)_{25}$[21] and $[Ir_{12}(CO)_{26}]^{2-}$[22] displaying 160 and 162 CVE, respectively. In contrast, $[Co_8Pt_4C_2(CO)_{24}]^{2-}$ exhibits an electron count of 170 CVE, close to those of the isostructural $[Co_{10}Rh_2N_2(CO)_{24}]^{2-}$ (168 CVE), $[Co_{11}RhN_2(CO)_{24}]^{2-}$ (168 CVE),[13] and $[Fe_6Ni_6N_2(CO)_{24}]^{n-}$ ($n = 2-4$) (168−170 CVE)[12] species.

Regarding the stereochemistry of the CO ligands, 12 are terminal (one per metal atom) and 12 bridge between the outer and the inner triangles. These bridging carbonyls are actually asymmetric, showing the shortest contacts with the outer all-Co triangles.

The structure of the paramagnetic monoanion $[1]^{-\bullet}$ has been determined on its $[NMe_3(CH_2Ph)][Co_{8-x}Pt_{4+x}C_2(CO)_{24}]$ ($x = 0,1$) salt, and it is almost overlapping with the one described above for the parent dianion. The elimination of one electron does not seem to affect significantly the M−M and M−C distances nor the CO stereochemistry. The unit cell contains two cluster anions and two $[NMe_3(CH_2Ph)]^+$ cations. Only two Co atoms, two M positions (disordered Co and Pt), one interstitial C atom, and seven CO ligands of the cluster anion are present within the asymmetric unit; all other atoms are generated by symmetry operations. The positions occupied by M(1) and M(2), which describe the inner octahedron, are disordered Co and Pt. A free refinement of the two independent M positions in the crystal structure of the $[NMe_3(CH_2Ph)][Co_{8-x}Pt_{4+x}C_2(CO)_{24}]$ ($x = 0,1$) salt results in a Co/Pt ratio of 7.82/4.18, which would correspond to a $[1]^{-\bullet}/[3]^-$ ratio in the crystal of ca. 4.55. Such a ratio is in good agreement with the one inferred from the ESI mass spectrum of the same crystals (4.5). The presence of $[3]^-$ within the crystal is probably unavoidable owing to the identical charge and structure of the $[1]^{-\bullet}$ and $[3]^-$ species, which leads to identical solubility properties of the two salts.

2.3. Electrochemical Studies. The redox activity of a crystalline sample of the dianion $[1]^{2-}$ in THF solution is illustrated in Figure 3.

In the cyclic voltammetric time scale, the dianion $[1]^{2-}$ undergoes two reduction processes possessing features of chemical reversibility ($E^{\circ\prime} = -0.91$ and -1.38 V, respectively; V vs SCE) and an oxidation process ($E^\circ = +0.18$ V) also having features of chemical reversibility. The anodic process is followed

(18) (a) Femoni, C.; Kaswalder, F.; Iapalucci, M. C.; Longoni, G.; Mehlstäubl, M.; Zacchini, S. *Chem. Commun.* **2005**, 5769. (b) Femoni, C.; Kaswalder, F.; Iapalucci, M. C.; Longoni, G.; Mehlstäubl, M.; Zacchini, S.; Ceriotti, A. *Angew. Chem., Int. Ed.* **2006**, *45*, 2060. (c) Femoni, C.; Kaswalder, F.; Iapalucci, M. C.; Longoni, G.; Zacchini, S. *Eur. J. Inorg. Chem.* **2007**, 1483.

(19) (a) Calabrese, J. C.; Dahl, L. F.; Chini, P.; Longoni, G.; Martinengo, S. *J. Am. Chem. Soc.* **1974**, *96*, 2614. (b) Longoni, G.; Chini, P. *J. Am. Chem. Soc.* **1976**, *98*, 7225. (c) Ceriotti, A.; Longoni, G.; Marchionna, M. *Inorg. Synth.* **1989**, *26*, 316.

(20) (a) Mingos, D. M. P. *Acc. Chem. Res.* **1984**, *17*, 311. (b) Wade, K. In *Transition Metal Clusters*; Jonhson, B. F. G., Eds.; Wiley and Sons: Chichester, UK, 1980; pp 193−264. (c) Mingos, D. M. P.; Wales, D. J. *Introduction to Cluster Chemistry*; Prentice-Hall: Englewood Cliffs, NJ, 1990.

(21) Ciani, G.; Sironi, A.; Martinengo, S. *Chem. Commun.* **1985**, 1757.

(22) Della Pergola, R.; Demartin, F.; Garlaschelli, L.; Manassero, M.; Martinengo, S.; Sansoni, M. *Inorg. Chem.* **1987**, *26*, 3487.

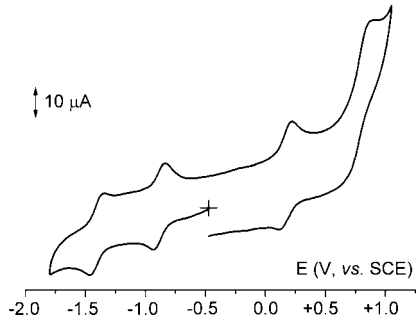

Figure 3. Cyclic voltammetric response recorded at a glassy carbon electrode in THF solution of crystalline $[NMe_3(CH_2Ph)]_2$**[1]** (1.2×10^{-3} M). $[NBu_4][PF_6]$ (0.2 M) supporting electrolyte. Scan rates 0.2 V s^{-1}.

by a further substantially irreversible oxidation ($E_p = +0.85$ V, at 0.2 V s^{-1}) partially overlapping the solvent discharge.

Controlled potential coulometric tests in correspondence of the first anodic process ($E_w = +0.45$ V) proved that it involves one electron per molecule. In spite of the clear features of chemical reversibility of such process, analysis of the cyclic voltammograms with scan rates progressively increasing from 0.02 to 5.00 V s^{-1} indicates that it is coupled to some slow chemical complications.[23] In fact, (i) the current ratio i_{pc}/i_{pa} at the lowest scan rate is slightly lower than 1 (about 0.8−0.9) but rapidly increases to 1.0; (ii) the current function $i_{pc}/v^{1/2}$ remains essentially constant; (iii) the peak-to-peak separation tends to depart from the theoretical value of 57 mV expected for a one-electron process, increasing progressively from 78 to 160 mV. As a matter of fact, such a finding is in agreement with the results of the chemical oxidation, which is coupled to the generation of minor amounts of $[Co_7Pt_5C_2(CO)_{24}]^-$ (**[3]**$^-$).

As far as the two reductions are concerned, based on the fact that their peak height is quite comparable with that of the one-electron oxidation, they are confidently assigned as one-electron processes. The respective diagnostic parameters indicate that in the time scale of cyclic voltammetry they involve simple electron transfers according to the formation of **[1]**$^{3-}$ and **[1]**$^{4-}$.

2.4. EPR Studies of [1]$^{2-}$ and [1]$^{-\bullet}$. The paramagnetic nature of the odd electrons **[1]**$^{-\bullet}$ is confirmed by EPR analyses. The spectrum at 290 K shows a very broad and weak signal around $g = 2$; however, the intensity of the signal gradually increases by decreasing the temperature, revealing the presence of an $S = 1/2$ system with $g_x = 1.90$, $g_y = 1.95$, and $g_z = 2.14$ at 5 K (Figure 4A at Q-band and 4B at W-band). These data agree with the presence of one unpaired electron in **[1]**$^{-\bullet}$ and a quasi-cylindrical symmetry of the molecule ($g_x \approx g_y \neq g_z$). In the spectra at 5 K (Figure 4A,B), it is possible to detect some minor irregular features around the main peaks. They are due to a noncomplete randomization of the powder; in fact, they change position and dimension by turning the sample. This confirms that no hyperfine coupling to ^{195}Pt ($I = 1/2$, 33.8%) and ^{59}Co ($I = 7/2$, 100%) is detected. It is noteworthy that the EPR spectra registered at the Q-band below 10 K display beside the major features due to the $S = 1/2$ **[1]**$^{-\bullet}$, some other very broad and weak peaks in the range of 0−1.6 T (Figure 4C). These become too broad to be observed at W-band, hampering a detailed analysis at this frequency. Nonetheless, the main peaks seem to be satisfactorily interpreted by simulating a system with $S = 1$, $g = 2.17$, and $D = 0.29$ cm^{-1} in the Q-band spectrum.

(23) Zanello, P. *Inorganic Electrochemistry. Theory, Practice and Application*; RSC: London, 2003.

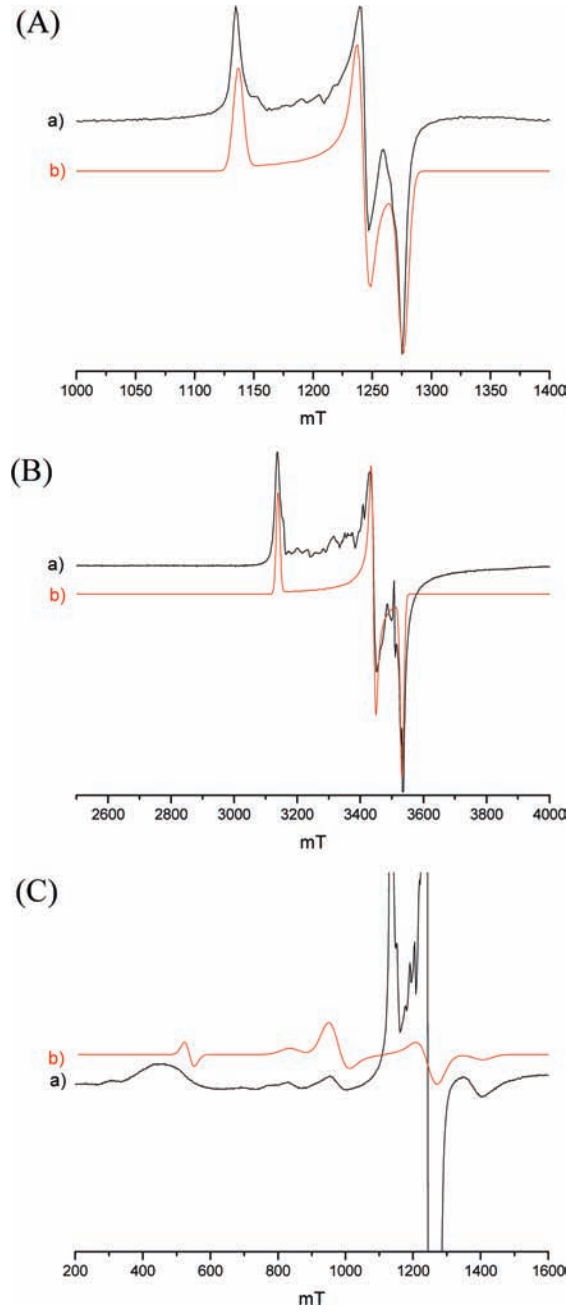

Figure 4. EPR spectra of **[1]**$^{-\bullet}$ as ground crystals registered at the Q-band (34.0 GHz) at 5 K (A), W-band (94 GHz) at 5 K (B), Q-band at 5 K showing the weak features (C) [(a) experimental (black) and (b) simulation (red)]. Experimental spectra are compared with the ones simulated for the $S = 1/2$ doublet state of **[1]**$^{-\bullet}$ in (A) and (B), whereas the weak features in (C) are zoomed in and compared to a simulated $S = 1$ state tentatively assigned to minor amount of the even-electron **[3]**$^-$.

This $S = 1$ signal may be tentatively assigned to the even-electron species **[3]**$^-$ present within the crystals of **[1]**$^{-\bullet}$ as described in section 2.2. We cannot exclude the presence of other unrecognized complexes in the spectrum; see the broad signal around 450 mT.

It is worth noting that the low-temperature EPR spectrum of the structurally related even-electron nitride $[Co_{10}Rh_2N_2(CO)_{24}]^{2-}$ [13] displayed the presence of a broad feature, which was interpreted as suggestive of population of a triplet state of the dianion. Moreover, DFT calculations on the related species $[Fe_6Ni_6N_2(CO)_{24}]^{n-}$ ($n = 2-4$)[12] and $[Co_{10}Rh_2N_2(CO)_{24}]^{2-}$ [13]

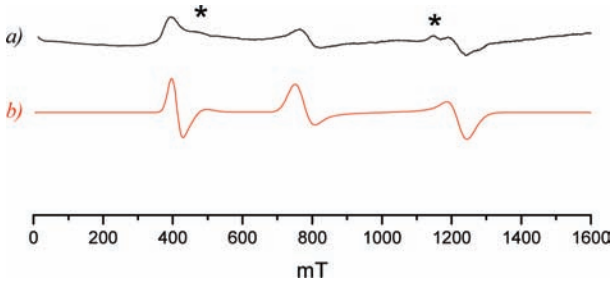

Figure 5. EPR spectra of $[\mathbf{1}]^{2-}$ as ground crystals at the Q-band at 5 K (a) and simulated spectrum (b) (* background impurity).

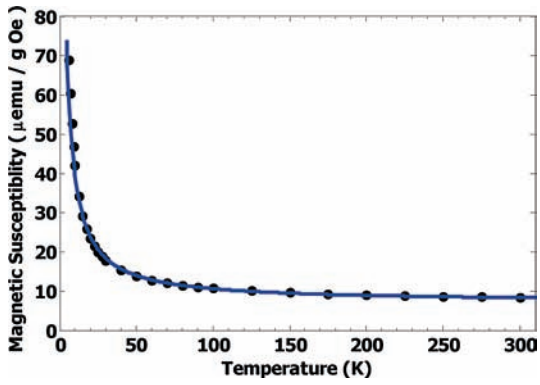

Figure 6. Temperature dependence of magnetization for $[NMe_3(CH_2Ph)]_2$**[1]** (ground crystals), in an applied field of 1 kOe. Data are black dots, the solid line represents the best-fitting curve from least-squares analysis (see text).

gave further support to the fact that their ground states could actually be a triplet state.

These considerations prompted an EPR study also of the parent even-electron $[\mathbf{1}]^{2-}$ dianion. The spectra at room temperature only display uninformative weak and broad features, probably due to background impurities. The EPR spectrum becomes more evident and informative at 5 K (Figure 5), which is satisfactorily reproduced by simulating a triplet state with $S = 1$, $g_x = g_y = 2.37$, $g_z = 2.75$, and $D = 0.5$ cm^{-1}. The observed triplet system is significantly different from that previously attributed to $[\mathbf{3}]^-$ and can be confidently attributed to the $[\mathbf{1}]^{2-}$ dianion. Furthermore, it is important to notice that there is no evidence in the EPR of the presence of the odd-electron $[\mathbf{1}]^{-\bullet}$ monoanion.

In conclusion, all isostructural $[\mathbf{1}]^{2-}$, $[\mathbf{3}]^-$, $[Co_{10}Rh_2N_2(CO)_{24}]^{2-}$,[13] and $[Fe_6Ni_6N_2(CO)_{24}]^{2-}$ [12] species possessing an even number of electrons appear to show a $S = 1$ triplet state, independently from the metal composition and the interstitial heteroatom.

2.5. SQUID Measurements. In order to clarify the characteristics of its triplet state, the even-electron system $[\mathbf{1}]^{2-}$ was further investigated performing dc SQUID magnetometry on ground crystalline samples of $[NMe_3(CH_2Ph)]_2$**[1]**. These analyses confirmed the paramagnetic nature of the compound, as it is evident from the Curie-like behavior of the temperature dependence of magnetization (Figure 6).

In addition to TDP, a TIP contribution is clearly evident in Figure 6: magnetization curves at 300 K point out that this is a ferromagnetic signal, with a saturation magnetization of 9.19(1) memu/g, probably arising from impurities (approximately equivalent to 50 ppm of iron).

In order to gain some insights into the paramagnetic properties of the cluster, magnetization curves $M(H)$ at low temperatures

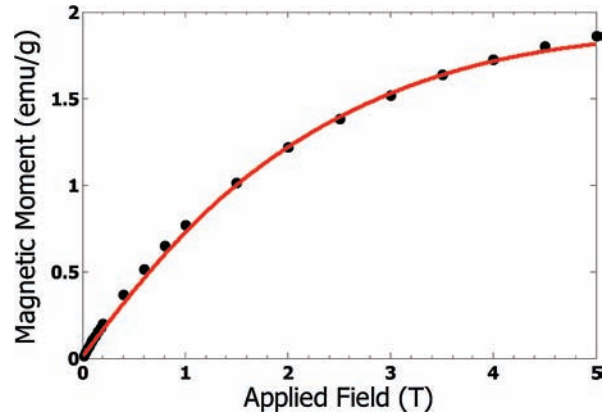

Figure 7. First magnetization curve for $[NMe_3(CH_2Ph)]_2$**[1]** (ground crystals) at 2 K. Data are black dots, the solid line represents the best-fitting curve from least-squares analysis (see text).

were recorded (Figure 7). On the basis of EPR results, which suggested the existence of a triplet state $S = 1$ with anisotropic g factor, fit of these data was performed considering a simple magnetic model, which even if it does not include any anisotropic term, accounts for all the essential magnetic features displayed by this system. In particular, (i) the contribution from orbital angular momentum was considered, using an isotropic Landé factor $g = 2.48$, calculated as the average over the EPR tensor parameters; (ii) beyond the ground state $S = 1$, an excited state with higher magnetization $S = 2$ was included, in order to account for the magnetization in the high field region ($H >$ 3 T), which is higher than the expected value for a simple $S =$ 1 system.

With these contributions, the average value of magnetization, calculated according to Boltzmann statistics, is

$$\langle M\rangle = \frac{Ng\mu_B}{Z}\left[\sum_{m=-1}^{1} m\exp(-\beta g\mu_B mH) + \exp(-\beta\Delta E)\sum_{m=-2}^{2} m\exp(-\beta g\mu_B mH)\right]$$

Here N is the number of molecules, Z is the partition function, and ΔE is the energy gap between the $S = 1$ state and the $S =$ 2 excited state. Least-square analysis of the low-temperature magnetization curve allowed an estimate of this energy gap as $\Delta E = 0.29(1)$ meV.

Fit of the temperature dependence of magnetization was also performed according to the given expression for $\langle M\rangle$ and evidenced that only approximately one-fourth of the molecules contribute to the paramagnetic signal. Thus, it is possible to conclude that in the solid compound $[NMe_3(CH_2Ph)]_2$**[1]** a fraction (25%) of the $[\mathbf{1}]^{2-}$ molecules is in a $S = 1$ ground state, while the remaining fraction (75%) is in a $S = 0$ ground state and does not contribute to the magnetic signal. It is worth noticing that the molecules in the $S = 1$ ground state can easily reach the $S = 2$ excited state, being separated by a small energy gap of only 0.29 meV; on the contrary, the excited states for the molecules in the null spin ground state are not accessible in the investigated temperature range (up to 300 K). The fact that within the crystals of $[\mathbf{1}]^{2-}$ the cluster molecules seem to have different electronic ground states ($S = 0$ and $S = 1$) is probably due to local deformations of the structure of the cluster (X-ray crystallographic analyses, in fact, give an average structure over several unit cells) which lead to spin-crossover.

DFT single-point energy calculations have been performed by means of the Gaussian 03 series of programs,[24] on different electronic states of **[1]**$^{2-}$ (S = 0, 1, 2, 3) leading to no clear conclusion (see Supporting Information for further details) since the calculated relative energies of the different electronic states considerably change by using different crystallographic coordinates and/or different basis sets.

3. Conclusions

In summary, the first examples of heterobimetallic Co−Pt dicarbide clusters have been prepared, showing C atoms encapsulated within expanded Co_4Pt_2 noncontiguous octahedral cages. These do not structurally resemble the so far known Co−Ni dicarbide congeners, viz. $[Co_6Ni_2C_2(CO)_{16}]^{2-}$, $[Co_6Ni_2C_2(CO)_{14}(CH_3CN)_2]^{2-}$, $[Co_3Ni_7C_2(CO)_{15}]^{3-}$, $[Co_3Ni_7C_2(CO)_{16}]^{2-}$,[25,26] in which the interstitial C atoms are lodged in contiguous trigonal prismatic cavities and close up to C−C bond distance (1.43−1.49 Å). They are rather isostructural with Co−Rh and Fe−Ni dinitrides. The **[1]**$^{2-}$ cluster is electron-rich possessing 170 CVE, rather than 168 as the $[Fe_6Ni_6N_2(CO)_{24}]^{2-}$ [12] and $[Co_{10}Rh_2N_2(CO)_{24}]^{2-}$ dinitrides,[13] and is isoelectronic with $[Fe_6Ni_6N_2(CO)_{24}]^{4-}$.[12] The weakening of the intralayer M−M interactions of the inner triangles may result into clustering of energy levels at the frontier region of the cluster, which triggers redox aptitude, as pointed out by their chemical and electrochemical behavior. As a further and more interesting consequence, triplet states of both 168 (viz. $[Fe_6Ni_6N_2(CO)_{24}]^{2-}$ [12] and $[Co_{10}Rh_2N_2(CO)_{24}]^{2-}$)[13] and 170 CVE (viz. **[1]**$^{2-}$ and **[3]**$^{-}$) species become comparable in energy with the singlet states and can be significantly populated. Indeed, all structurally characterized species reported in this paper (i.e., **[1]**$^{2-}$, **[3]**$^{-}$, and **[1]**$^{-\bullet}$) are magnetic. In the latter case, the paramagnetism is due to the presence of one unpaired electron in the SOMO, resulting in a S = 1/2 doublet state. Conversely, the paramagnetic behavior displayed by the even-electron species **[1]**$^{2-}$ and **[3]**$^{-}$ arises from S = 1 triplet states, as indisputably pointed out by their EPR spectra. The EPR spectrum of **[1]**$^{2-}$ excludes any possible contamination of the sample by the odd-electron **[1]**$^{-\bullet}$ monoanion and gives extreme confidence to the measured magnetic susceptibility. SQUID measurements are in keeping with the fact that some cluster molecules within the crystals of **[1]**$^{2-}$ are in a S = 1 ground state (25%), whereas the remainder are in a S = 0 ground state. Taking into account the relatively low nuclearity of these clusters, it seems justified to conclude that magnetic properties may develop in TMCC owing to progressive metallization as the cluster size increases (e.g., $[Ni_{16}Pd_{16}(CO)_{40}]^{4-}$),[27] even if the magnetic properties of the title compounds are yet likely triggered by ad hoc conditions. In any case, the presently reported indisputable examples of intrinsic magnetism of even-electron TMCC may lend support to the authenticity of some previously ascertained magnetism of highest nuclearity TMCC and gold colloidal particles. The development of electronic and magnetic properties in molecular TMCCs make them candidates for applications in nanoscience and nanotechnologies as molecular nanocapacitors, superparamagnetic quantum dots, and nanomagnets,[28] as well as precursors of narrow dispersed magnetic alloy and metal oxide nanoparticles of corresponding composition.[29,30]

4. Experimental Section

4.1. General Procedures. All reactions and sample manipulations were carried out using standard Schlenk techniques under nitrogen and in dried solvents. All reagents were commercial products (Aldrich) of the highest purity available and used as received. The $[NR_4]_2[Co_6C(CO)_{15}]$ [NR_4 = NMe_4, $NMe_3(CH_2Ph)$][15] and $PtCl_2(Et_2S)_2$[31] salts have been prepared according to the literature. Analysis of Co and Pt was performed by atomic absorption on a Pye-Unicam instrument. Analyses of C, H, and N were obtained with a ThermoQuest FlashEA 1112NC instrument. IR spectra were recorded on a Perkin-Elmer SpectrumOne interferometer in CaF_2 cells. ESI mass spectra were recorded on a Waters Micromass ZQ4000 instrument. ^{13}C NMR spectra have been recorded on a Varian Mercury 400 MHz spectrometer and referenced to internal TMS.

Cyclic voltammetry was performed in a three-electrode cell containing a gold or a glassy carbon working electrode surrounded by a platinum spiral counter electrode and an aqueous saturated calomel reference electrode (SCE) mounted with a Luggin capillary. A BAS 100 W electrochemical analyzer was used as the polarizing unit. All of the potential values are referred to the saturated calomel electrode (SCE). Under the present experimental conditions, the one-electron oxidation of ferrocene occurs at $E^{\circ\prime}$ = +0.59 V in THF solution. Controlled potential coulometry was performed in an H-shaped cell with anodic and cathodic compartments separated by a sintered glass disk. The working macroelectrode was a platinum gauze; a mercury pool was used as the counter electrode. Anhydrous 99.9% HPLC-grade tetrahydrofuran (Aldrich) was distilled in the presence of sodium before use. Fluka $[NBu_4][PF_6]$ (electrochemical grade) was used as supporting electrolytes.

Magnetic susceptibility measurements were performed on ground crystals with a Quantum Design MPMS XL SQUID magnetometer, capable of fields as high as 5 T. Samples for SQUID measurements were prepared in a glovebox.

Structures have been drawn with SCHAKAL99.[32]

4.2. Synthesis of $[NMe_4]_2$[1]·2THF. $PtCl_2(Et_2S)_2$ (0.95 g, 2.13 mmol) was added in portions to a solution of $[NMe_4]_2[Co_6C(CO)_{15}]$ (1.03 g, 1.03 mmol) in THF (30 mL) with stirring. The mixture was left to react for 3 days, until all of the starting $[NMe_4]_2[Co_6C(CO)_{15}]$ had disappeared by IR monitoring, and then, the resulting dark green solution was evaporated to dryness. The residue was washed with water (40 mL) and toluene (30 mL) and extracted in THF (30 mL), resulting in a dark green solution of the crude compound. Precipitation by slow diffusion of hexane (60 mL) gave a dark-green crystalline precipitate composed of crystals of $[NMe_4]_2$**[2]**·2THF (yield 1.15 g, 59.5% based on Co, 86.6% based on Pt). The salt is soluble in THF and acetone; in more polar solvents, it slowly decomposes: IR (THF, 293 K) ν(CO) 2014(s), 1826(m) cm^{-1}; ESI-MS (THF) ES m/z (relative intensity in parentheses) 974 (100) $[Co_8Pt_4C_2(CO)_{24}]^{2-}$; 1947 (15) $[Co_8Pt_4C_2(CO)_{24}]^{-}$. Anal. Calcd for $C_{42}H_{40}Co_8N_2O_{26}Pt_4$ (2240.54): C, 22.52;

(24) Frisch, M. J. *Gaussian 03*, revision D.01; Gaussian Inc.: Wallingford, CT, 2004.
(25) (a) Arrigoni, A.; Ceriotti, A.; Della Pergola, R.; Longoni, G.; Manassero, M.; Masciocchi, M.; Sansoni, M. *Angew. Chem., Int. Ed. Engl.* **1984**, *23*, 322. (b) Ceriotti, A.; Della Pergola, R.; Garlaschelli, L.; Longoni, G.; Manassero, M.; Masciocchi, M.; Sansoni, M.; Zanello, P. *Gazz. Chim. Ital.* **1992**, *122*, 365.
(26) (a) Longoni, G.; Ceriotti, A.; Della Pergola, R.; Manassero, M.; Perego, M.; Piro, G.; Sansoni, M. *Philos. Trans. R. Soc. London, Ser. A* **1982**, *308*, 47. (b) Arrigoni, A.; Ceriotti, A.; Della Pergola, R.; Longoni, G.; Manassero, M.; Sansoni, M. *J. Organomet. Chem.* **1985**, *196*, 243.
(27) Riccò, M.; Shiroka, T.; Carretta, S.; Bolzoni, F.; Femoni, C.; Iapalucci, M. C.; Longoni, G. *Chem.—Eur. J.* **2005**, *11*, 2856.
(28) Femoni, C.; Kaswalder, F.; Iapalucci, M. C.; Longoni, G.; Zacchini, S. *Coord. Chem. Rev.* **2006**, *250*, 1580.
(29) Rutledge, R. D.; Morris, W. H.; Wellons, M. S.; Gai, Z.; Shen, J.; Bentley, J.; Wittig, J. E.; Lukehart, C. M. *J. Am. Chem. Soc.* **2006**, *128*, 14210.
(30) Robinson, I.; Zacchini, S.; Tung, L. D.; Shinya, M.; Thanh, N. T. K. *Chem. Mater.* **2009**, *21*, 3021.
(31) Kauffmann, G. B.; Corvan, D. O. *Inorganic Synthese*; Wiley: New York, 1960; Collect. Vol. VI, p 211.
(32) Keller, E. *SCHAKAL99*; University of Freiburg: Freiburg, Germany, 1999.

Table 2. Crystal Data and Experimental Details for $[NMe_4]_2$**[1]**·2THF, $[NMe_3(CH_2Ph)]_2$**[1]**·2THF·$0.5CH_3C_6H_5$, and $[NMe_3(CH_2Ph)][Co_{8-x}Pt_{4+x}C_2(CO)_{24}]$ ($x = 0,1$)

	$[NMe_4]_2$**[1]**·2THF	$[NMe_3(CH_2Ph)]_2$**[1]**·2THF·$0.5CH_3C_6H_5$	$[NMe_3(CH_2Ph)][Co_{8-x}Pt_{4+x}C_2(CO)_{24}]$ ($x = 0,1$)
formula	$C_{42}H_{40}Co_8N_2O_{26}Pt_4$	$C_{57.5}H_{52}Co_8N_2O_{26}Pt_4$	$C_{36}H_{16}Co_{7.82}NO_{24}Pt_{4.18}$
Fw	2240.52	2438.81	2122.81
T, K	291(2)	293(2)	293(2)
λ, Å	0.71073	0.71073	0.71073
crystal system	monoclinic	monoclinic	monoclinic
space group	*C*2/*c*	$P2_1/c$	*C*2/*m*
a, Å	24.610(2)	11.1326(4)	19.0519(13)
b, Å	11.1558(9)	30.3345(11)	11.7160(8)
c, Å	22.8484(19)	21.2296(8)	11.4645(8)
β, °	111.649(10)	99.7220(10)	104.8140(10)
cell volume, Å^3	5830.4(8)	7066.3(4)	2474.0(3)
Z	4	4	2
D_c, g cm^{-3}	2.553	2.292	2.850
μ, mm^{-1}	11.846	9.785	14.394
F(000)	4168	4588	1936
crystal size, mm	0.19 × 0.15 × 0.11	0.19 × 0.14 × 0.11	0.22 × 0.15 × 0.14
θ limits, °	1.92−25.99	1.18−27.00	1.84−27.99
index ranges	$-30 \times h \times 30$	$-14 \times h \times 14$	$-25 \times h \times 24$
	$-13 \times k \times 13$	$-38 \times k \times 38$	$-15 \times k \times 15$
	$-28 \times l \times 28$	$-27 \times l \times 27$	$-15 \times l \times 15$
reflections collected	29365	78839	14331
independent reflections	5743 [$R_{int} = 0.0335$]	15429 [$R_{int} = 0.0898$]	3094 [$R_{int} = 0.0259$]
completeness to θ max	99.9%	99.9%	98.7%
data/restraints/parameters	5743/ 85/373	15429/479/845	3094/91/225
goodness on fit on F^2	1.030	1.020	1.056
R_1 ($I > 2\sigma(I)$)	0.0431	0.0607	0.0221
wR_2 (all data)	0.1192	0.1818	0.0503
largest diff. peak and hole, e Å^{-3}	2.997/−2.534	1.810/−1.492	1.149/−0.915

H, 1.80; N, 1.25; Co, 21.04; Pt, 34.83. Found: C, 22.81; H, 1.65; N, 1.37; Co, 20.92; Pt, 35.01.

Crystals of the related $[NMe_3(CH_2Ph)]_2$**[1]**·2THF·$0.5CH_3C_6H_5$ were obtained following the same procedure as above employing $[NMe_3(CH_2Ph)]_2[Co_6C(CO)_{15}]$ and layering toluene instead of hexane.

4.3. Synthesis of $[NMe_3(CH_2Ph)][Co_{8-x}Pt_{4+x}C_2(CO)_{24}]$ ($x = 0,1$). I_2 (0.0751 g, 0.296 mmol) was added to a solution of $[NMe_3(CH_2Ph)]_2$**[1]**·2THF·$0.5CH_3C_6H_5$ (1.21 g, 0.496 mmol) in THF (30 mL) with stirring. The mixture was left to react for 2 h, up to complete reaction as monitored by IR spectroscopy. The solvent was, then, removed in vacuum, and the residue was washed with water (40 mL) and toluene (30 mL) and extracted in CH_2Cl_2 (20 mL). Precipitation by slow diffusion of hexane (50 mL) gave a black crystalline precipitate composed of crystals of $[NMe_3(CH_2Ph)][Co_{8-x}Pt_{4+x}C_2(CO)_{24}]$ ($x = 0,1$) (yield 0.78 g, 75.0%). The salt is soluble in THF, CH_2Cl_2, and acetone: IR (THF, 293 K) ν(CO) 2040(s), 1849(m) cm^{-1}; (CH_2Cl_2, 293 K) ν(CO) 2042(s), 1848(m) cm^{-1}; ESI-MS (THF) ES *m*/*z* (relative intensity in parentheses) 974 (35) $[Co_8Pt_4C_2(CO)_{24}]^{2-}$; 1947 (100) $[Co_8Pt_4C_2(CO)_{24}]^-$; 2084 (30) $[Co_7Pt_5C_2(CO)_{24}]^-$. Anal. Calcd for $C_{36}H_{16}Co_{7.82}NO_{24}Pt_{4.18}$ (2122.81): C, 20.37; H, 0.76; N, 0.66; Co, 21.71; Pt, 38.41. Found: C, 20.48; H, 0.62; N, 0.79; Co, 21.95; Pt, 38.19.

4.4. EPR Measurements. The spectra of **[1]**$^{2-}$ and **[1]**$^{-\bullet}$, as their crystalline $[NMe_3(CH_2Ph)]_2$**[2]**·2THF·$0.5CH_3C_6H_5$ and $[NMe_3(CH_2Ph)][Co_{8-x}Pt_{4+x}C_2(CO)_{24}]$ salts, respectively, have been recorded at the Q-band (34.0 GHz) on an Elexsys E500 Bruker spectrometer from 295 to 5 K using 1.0 mW power, 0.5 mT modulation amplitude, and 100 kHz modulation frequency; at the W-band (94.0 GHz) on an Elexsys E600 Bruker spectrometer at 5 K using 4.8×10^{-3} mW power, 0.5 mT modulation amplitude, and 100 kHz modulation frequency. The samples for the measurements were prepared by grinding pure crystals of **[1]**$^{-\bullet}$ and **[1]**$^{2-}$ and transferring the powders to the EPR tube under nitrogen atmosphere.

EPR simulations were performed using the program XSophe version 1.1.4.

4.5. X-ray Crystallographic Study. Crystal data and collection details for $[NMe_4]_2$**[1]**·2THF, $[NMe_3(CH_2Ph)]_2$**[1]**·2THF·$0.5CH_3C_6H_5$, and $[NMe_3(CH_2Ph)][Co_{8-x}Pt_{4+x}C_2(CO)_{24}]$ ($x = 0,1$) are reported in Table 2. The diffraction experiments were carried out on a Bruker APEX II diffractometer equipped with a CCD detector using Mo Kα radiation. Data were corrected for Lorentz polarization and absorption effects (empirical absorption correction SADABS).[33] Structures were solved by direct methods and refined by full-matrix least-squares based on all data using F^2.[34] Hydrogen atoms were fixed at calculated positions and refined by a riding model. All non-hydrogen atoms were refined with anisotropic displacement parameters, unless otherwise stated.

$[NMe_4]_2$[1]·2THF: The unit cell contains four cluster anions (located on an inversion center), eight $[NMe_4]^+$ cations, and eight THF molecules. The positions occupied by M(4), M(5), and M(6) are disordered Co and Pt. Dummy atom constrains (instructions EXYZ and EADP in SHELXL) were used during refinement for these positions, and a free variable was assigned to each position. The overall composition of the cluster was restrained to be in the ratio Co/Pt = 8:4 on the basis of ESI-MS analyses. The restrained free variables refined as follows: 0.79965 Pt(4), 0.63872 Pt(5), 0.56087 Pt(6) [Co occupancy factors are the complement at one of each free variable]. A refinement without compositional restraints gave 0.71881 Pt(4), 0.56601 Pt(5), 0.49337 Pt(6) [Co/Pt = 8.44: 3.56]. Similar *U* restraints (su = 0.01) were applied to the C and O atoms. Restraints to bond distances were applied as follow: 1.47 Å (su = 0.02) for C−N in $[NMe_4]^+$; 1.43 Å (su = 0.01) for C−O; and 1.53 Å (su = 0.01) for C−C in THF.

$[NMe_3(CH_2Ph)]_2$[1]·2THF·$0.5CH_3C_6H_5$: The unit cell contains four cluster anions, eight $[NMe_3(CH_2Ph)]^+$ cations, eight THF molecules (all located on a general positions), and two toluene molecules (located on an inversion center). The positions occupied by M(1), M(2), M(3), M(4), M(5), and M(6) are disordered Co and Pt. Dummy atom constrains (instructions EXYZ and EADP in SHELXL) were used during refinement for these positions, and a free variable was assigned to each position. The overall composition

(33) Sheldrick, G. M. *SADABS, Program for empirical absorption correction*; University of Göttingen: Göttingen, Germany, 1996.
(34) Sheldrick, G. M. *SHELX97, Program for crystal structure determination*; University of Göttingen: Göttingen, Germany, 1997.

of the cluster was restrained to be in the ratio Co/Pt = 8:4 on the basis of ESI-MS analyses. The restrained free variables refined as follows: 0.85510 Pt(1), 0.83742 Pt(2), 0.79170 Pt(3), 0.73567 Pt(4), 0.47164 Pt(5), and 0.30775 Pt(6) [Co occupancy factors are the complement at one of each free variable]. A refinement without compositional restraints gave 0.72933 Pt(1), 0.71188 Pt(2), 0.67111 Pt(3), 0.62034 Pt(4), 0.37342 Pt(5), and 0.22612 Pt(6) [Co/Pt = 8.67:3.33]. The toluene molecule is disordered over two symmetry related (by inversion) positions; the independent image of the molecule was refined isotropically with 0.5 occupancy factor. Similar *U* restraints (su = 0.005) were applied to the C and O atoms. Restraints to bond distances were applied as follows: 1.47 Å (su = 0.01) for C−N and 1.51 Å (su = 0.01) for C−C (nonaromatic) in $[NMe_3(CH_2Ph)]^+$; 1.43 Å (su = 0.01) for C−O and 1.53 Å (su = 0.01) for C−C in THF. The aromatic atoms of the disordered toluene molecule were fitted to a regular hexagon (AFIX 66 instruction in SHELXL).

$[NMe_3(CH_2Ph)][Co_{8-x}Pt_{4+x}C_2(CO)_{24}]$ (x = 0,1). The unit cell contains two cluster anions and two $[NMe_3(CH_2Ph)]^+$ cations. Only two Co atoms, two M positions (disordered Co and Pt), one interstitial C atom, and seven CO ligands of the cluster anion are present within the asymmetric unit; all other atoms are generated by symmetry operations. The positions occupied by M(1) and M(2) are disordered Co and Pt. Dummy atom constrains (instructions EXYZ and EADP in SHELXL) were used during refinement for these positions, and a free variable was assigned to each position. Since in this case ESI-MS analyses indicated the presence of a mixture of $[Co_8Pt_4C_2(CO)_{24}]^-$ and $[Co_7Pt_5C_2(CO)_{24}]^-$ in 4.5:1 ratio, differently from the previous cases, no restraints on the composition were applied. This free refinement gave the following occupancy factors: 0.97711 Pt(1), 0.13594 Pt(2) [Co occupancy factors are the complement at one of each free variable] corresponding to the composition Co/Pt = 7.82:4.18. From this data, a **[1]**$^-$/**[3]**$^-$ ratio of 4.55 can be derived for the crystal structure, in good agreement with ESI-MS data. The $[NMe_3(CH_2Ph)]^+$ cation is disordered over four symmetry related (by 2 and *m*) positions; the independent image of the molecule was refined isotropically with 0.25 occupancy factor. Similar *U* restraints (su = 0.005) were applied to the C and O atoms.

Acknowledgment. We thank Prof. David Collison (University of Manchester) and Dr. Stefano Carretta (University of Parma) for fruitful discussion. We thank the Universities of Bologna (Project CLUSTERCAT), Siena, Parma, and MIUR (PRIN) for funding. We thank EPSRC (U.K.) for the EPR experiments.

Supporting Information Available: CIF files giving X-ray crystallographic data for the structure determinations of $[NMe_4]_2$**[1]**·2THF, $[NMe_3(CH_2Ph)]_2$**[1]**·2THF·0.5$CH_3C_6H_5$, and $[NMe_3(CH_2Ph)][Co_{8-x}Pt_{4+x}C_2(CO)_{24}]$ (x = 0,1). Experimental details on the synthesis and characterization of the compounds **[2]**$^{n-}$ (n = 2,3) and **[3]**$^-$. Details on EHMO and DFT calculations. Full reference for ref 24. Labeling for the disordered positions in $[NMe_3(CH_2Ph)]_2$**[1]**·2THF·0.5$CH_3C_6H_5$. This material is available free of charge via the Internet at http://pubs.acs.org.

JA907608C